Electronic Supplementary Material (ESI) for Dalton Transactions.

Supporting Information

A nitrogen-rich ligand as a scaffold for slow magnetic relaxation in dysprosium-based 0D and 1D architectures

*Gabriel Brunet, Elena Sebastiao, Tomasz G. Witkowski, Ilia Korobkov, Bulat Gabidullin and Muralee Murugesu**

Department of Chemistry and Biomolecular Sciences, University of Ottawa, 10 Marie Curie, Ottawa, ON K1N 6N5, Canada

Table of contents

Experimental section:

General considerations: All manipulations were performed under aerobic conditions using chemicals and solvents from commercial sources (Acros Organics, Fisher Scientific, Alfa Aesar, and Strem Chemicals) and used as received without further purification.

Synthesis of 2,3,5,6-Tetra(1*H*-tetrazol-5-yl)pyrazine (H_4TTP):

To a solution of pyrazine-2,3,5,6-tetracarbonitrile (20.0 mmol, 3.60 g) in 50 mL dimethyl sulfoxide, sodium azide (82.0 mmol, 5.34 g) is added in one portion. The mixture is stirred for 72 hours at 100 °C. Afterwards, the reaction mixture is poured onto ice and acidified with sulfuric acid. The obtained yellowish product is filtered, washed with water and then boiled in water for 0.5 h, the precipitate is filtered off and washed with water (yields 5.84 g, 83%). DSC (5 °C min^{-1}): 260 °C (dec.); ^{1}H NMR (300.00 MHz, dmso-d_6, ppm) δ: 7.16 (br., 4 H, N*H*); ^{13}C{^{1}H} NMR (75.0 MHz, dmso-d_6, ppm); MS (TOF-MS-ES−): m/z: 351.0794 $[M-\text{H}]^-$ (Exact Mass: 351.0788).

Synthesis of $[\text{Dy}(\text{H}_2\text{TTP})(\text{H}_2\text{O})_6]_2(\text{H}_2\text{TTP})_{0.5}\cdot 6\text{H}_2\text{O}$ (1a):

A mixture of $\text{DyCl}_3\cdot 6\text{H}_2\text{O}$ (32.3 mg, 0.086 mmol) and H_4TTP (15.0 mg, 0.043 mmol) were sonicated for 10 min in 3 mL of H_2O. The resulting solution was then transferred in a 20 mL Teflon-lined stainless steel vessel, sealed, and heated to 160 °C for 3 days, and slowly cooled to room temperature over a period of 24 hours (5.41 °C h^{-1}). Clean yellow block-like crystals were obtained with a yield of 18 %. Anal. Calcd for $\text{DyC}_{12}\text{H}_{27}\text{N}_{27}\text{O}_{12}$: C 15.94%; H 3.01%; N 41.93%. Found: C 16.49%; H 2.53%; N 42.10%. Selected IR (cm^{-1}): 3174 (br), 1645 (m), 1477 (m), 1418 (s), 1338 (m), 1282 (m), 1213 (w), 1184 (m), 1074 (s), 667 (br).

Synthesis of $[\text{Gd}(\text{H}_2\text{TTP})(\text{H}_2\text{O})_6]_2(\text{H}_2\text{TTP})_{0.5}\cdot 6\text{H}_2\text{O}$ (1b):

The same procedure as **1a** was replicated for **1b**, but replacing the metal salt with $\text{GdCl}_3\cdot 6\text{H}_2\text{O}$ (31.8 mg, 0.086 mmol). Colourless block-like crystals were obtained with a yield of 16 %. Anal. Calcd for $\text{GdC}_{12}\text{H}_{27}\text{N}_{27}\text{O}_{12}$: C 16.03%; H 3.03%; N 42.07%. Found: C 16.48%; H 2.62%; N 42.38%. Selected IR (cm^{-1}): 3175 (br), 1645 (m), 1477 (m), 1416 (s), 1338 (m), 1282 (m), 1213 (w), 1184 (m), 1073 (s), 666 (br).

Synthesis of $[\text{Dy}_2(\text{TTP})(\mu\text{-OH})_{1.3}(\mu\text{-HCOO})_{0.7}(\text{H}_2\text{O})_6]_n$ (2a):

A mixture of $\text{DyCl}_3\cdot 6\text{H}_2\text{O}$ (32.3 mg, 0.086 mmol), H_4TTP (15.0 mg, 0.043 mmol) and formic acid (16 µL, 0.424 mmol) were sonicated for 10 min in 3 mL of H_2O. The resulting solution was then transferred in a 20 mL Teflon-lined stainless steel vessel, sealed, and heated to 160 °C for 3 days, and slowly cooled to room temperature over a period of 24 hours (5.41 °C h^{-1}). Yellow-orange block-like crystals were obtained with a yield of 15 %. Anal. Cald for

$Dy_2C_{8.70}H_{14}N_{18}O_{8.70}$: C 12.51%; H 1.69%; N 30.19%. Found: C 12.67%; H 1.65%; N 29.05%. Selected IR (cm^{-1}): 3163 (br), 1666 (w), 1646 (m), 1641 (m), 1482 (m), 1305 (m), 1251 (m), 1234 (m), 1125 (m), 1049 (m), 680 (br).

Synthesis of $[Gd_2(TTP)(\mu\text{-}OH)_{1.25}(\mu\text{-}HCOO)_{0.75}(H_2O)_6]_n$ (2b):

The same procedure as **2a** was replicated for **2b**, but replacing the metal salt with $GdCl_3{\cdot}6H_2O$ (31.8 mg, 0.086 mmol). Yellow block-like crystals were obtained with a yield of 11 %. Anal. Cald for $Gd_2C_{8.75}H_{14}N_{18}O_{8.75}$: C 12.73%; H 1.71%; N 30.53%. Found: C 12.99%; H 1.70%; N 29.71%. Selected IR (cm^{-1}): 3165 (br), 1666 (w), 1646 (m), 1641 (m), 1483 (m), 1305 (m), 1251 (m), 1234 (m), 1125 (m), 1049 (m), 686 (br).

Single Crystal X-ray Diffraction

Single crystal X-ray diffraction data were collected at 200(2) K on Bruker Smart and Kappa Apex II CCD diffractometers with graphite-monochromatised Mo-K$_\alpha$ radiation. Data collection and processing were performed with the Bruker APEX II software packages.[1] Semi-empirical adsorption corrections based on equivalent reflections were applied.[2] The structures were solved by direct methods and refined with full-matrix least-squares procedures using SHELXL[3] and WinGX.[4] All non-hydrogen atoms were refined anisotropically. The positions of the hydrogen atoms were calculated based on the geometry of related non-hydrogen atoms.

In the crystal structures of **1a** and **1b** the H_2TTP^{2-} anion (C(9),…,N(36)) is located on an inversion centre and is disordered over two positions with equal occupancies fixed at 0.5. Due to the overlap of two positions, the molecule was refined with restraints on 1,2- and 1,3-distances (SAME command) and the H_2TTP molecule coordinated to Dy (C(1),…,N(18)) acted as an equivalent molecule. Enhanced rigid-bond restraints (RIGU command) were applied to the atomic displacement parameters of these two molecules.

All hydrogen atoms of water molecules were refined with U_{iso} constrained at $1.5U_{eq}$ of the corresponding oxygen atoms and with O-H bond lengths restrained at 0.82Å (DFIX command), except H(10D), H(11A), H(11B), H(11C) atoms in **1a** that were refined as ‘riding’ (AFIX command) on the corresponding oxygen atoms. In **1a** and **1b** the 1,3-distances in the water molecules were restrained to be mutually equal (SADI command). The O(1),…,O(8) water molecules were not disordered. The O(9),…,O(12) molecules were each modelled as disordered over two positions; the atomic displacement parameters were constrained to be equal (EADP command) due to the proximity/overlap of the positions. In **1a** the occupancy ratios were fixed at 0.5:0.5. In **1b** the occupancy ratios were not fixed and were refined to 0.536(5):0.464(5), 0.633(3):0.367(3), 0.498(3):0.502(3), 0.477(3):0.523(3), respectively. In **1a** and **1b** the hydrogen atoms H(14A), H(18A), H(25), H(32) of the N-H groups were refined using a riding model (AFIX command).

The structures of **2a** and **2b** show substitutional/occupancy disorder with a hydroxyl group and a formate anion sharing a common space. Their occupancy ratio was refined to about

0.65:0.35 (**2a**) and 0.625:0.375 (**2b**) and was fixed at the last stages of refinement. The hydrogen atoms of the hydroxyl group and the water molecules were refined using a riding model. The atomic displacement parameters of the formate were restrained in **2b** (SIMU and RIGU commands).

Table S1: Crystallographic Data for **1a**, **1b**, **2a** and **2b**.

Compound	**1a**	**1b**	**2a**	**2b**
Empirical Formula	$DyC_{12}H_{27}N_{27}O_{12}$	$GdC_{12}H_{27}N_{27}O_{12}$	$Dy_2C_{8.70}H_{14}N_{18}O_{8.70}$	$Gd_2C_{8.75}H_{14}N_{18}O_{8.75}$
Crystal system	Triclinic	Triclinic	Triclinic	Triclinic
Space group	P–1	P–1	P–1	P–1
a (Å)	9.7883(6)	9.8069(5)	6.5214(2)	6.5239(2)
b (Å)	11.1740(6)	11.2059(6)	7.8070(2)	7.8414(2)
c (Å)	14.3567(8)	14.4149(7)	10.6509(3)	10.6792(3)
α (°)	101.599(3)	97.8160(10)	104.2559(12)	104.2714(12)
β (°)	97.500(3)	93.9320(10)	97.5429(14)	97.0307(14)
γ (°)	93.781(3)	93.9320(10)	98.3219(15)	97.8719(13)
V (Å^3)	1518.14(15)	1528.97(14)	512.09(3)	517.48(3)
Z	2	2	1	1
ρ_{calc} (g cm^{-3})	1.978	1.952	2.708	2.650
λ (Å)	0.71073	0.71073	0.71073	0.71073
T (K)	200(2)	200(2)	200(2)	200(2)
μ (mm^{-1})	2.566	2.273	7.332	6.444
F (000)	900	896	394	390
Reflections Collected	17057	14787	5663	5574
Independent Reflections	7372	7516	2479	2524
Reflections with I > 2σ(I)	6864	7166	2408	2482
Goodness of fit on F^2	1.080	1.070	1.108	1.032
R_1, wR_2 ($I > 2\sigma(I)$)[a]	0.0263, 0.0621	0.0173, 0.0424	0.0243, 0.0559	0.0219, 0.588
R_1, wR_2 (all data)	0.0295, 0.0640	0.0187, 0.0429	0.0251, 0.0565	0.0223, 0.0591

[a] $R = R_1 = \sum||F_o| - |F_c||/\sum|F_o|$; $wR_2 = \{\sum[w(F_o^2 - F_c^2)^2]/\sum[w(F_o^2)^2]\}^{1/2}$; $w = 1/[\sigma^2(F_o^2)+(ap)^2 + bp]$, where $p = [\max(F_o^2,0) + 2F_c^2]/3$; and $Rw = [w(|F_o| - |F_c|)^2 / w|F_o|^2]^{1/2}$, where $w = 1/\sigma^2(|F_o|)$.

Infrared Spectroscopy

Infrared spectra were performed with a Varian 640 FTIR spectrometer equipped with an ATR in the 4000 cm^{-1} to 600 cm^{-1} range.

Magnetic measurements

Magnetic susceptibility measurements were performed using a MPMS-XL7 Quantum Design SQUID magnetometer. Direct current (dc) susceptibility measurements were performed at temperatures ranging from 1.9 to 300 K, and up to applied fields of 7 T. Measurements were performed on crushed polycrystalline samples of 10.4, 10.1, 11.4 and 10.5 mg for compounds **1a**, **1b**, **2a** and **2b**, respectively, and wrapped in a polyethylene membrane. Alternating current (ac) susceptibility measurements were performed under an oscillating ac field of 3.78 Oe and ac frequencies ranging from 0.1 to 1488 Hz. Magnetization vs. field measurements were performed at 100 K in order to check for the presence of ferromagnetic impurities, which were found to be absent in all samples. Magnetic data was corrected for diamagnetic contributions using Pascal's constants.

Electrostatic Potential

The molecular structure of H_4TTP was fully optimized without symmetry constraints to C_1 symmetry. The calculations of electrostatic potential (ESP) was performed applying the B3LYP/6-311+G(2d,p) level of theory using the Gaussian G09 program package.[5] The ESP of H_4TTP on the 0.001 electron·bohr^{-3} hypersurface with the colour range from red (V(r) ≤ –0.075 Hartree, electron-rich regions) to blue (V(r) ≥ +0.075 Hartree, electron-deficient regions) was illustrated using GaussView 5 software (Figure S14).[6]

Table S2: Select bond distances and angles of **1a** and **1b**.

Select bond distances (Å)			
Dy1-O1	2.387(2)	Gd1-O1	2.4211(13)
Dy1-O2	2.370(2)	Gd1-O2	2.3998(14)
Dy1-O3	2.387(2)	Gd1-O3	2.4188(13)
Dy1-O4	2.384(2)	Gd1-O4	2.4180(14)
Dy1-O5	2.384(2)	Gd1-O5	2.4129(13)
Dy1-N1	2.805(2)	Gd1-N1	2.8282(14)
Dy1-N3	2.494(2)	Gd1-N3	2.5217(14)
Dy1-N7	2.524(2)	Gd1-N7	2.5494(14)
Select angles (°)			
N3-Dy1-N1	60.47(7)	N3-Gd1-N1	60.07(4)
N7-Dy1-N1	59.70(7)	N7-Gd1-N1	59.46(4)

Table S3: Select bond distances and angles of **2a** and **2b**.

Select bond distances (Å)			
Dy1-O1	2.323(3)	Gd1-O1	2.353(3)
Dy1-O2	2.380(3)	Gd1-O2	2.413(3)
Dy1-O3	2.333(3)	Gd1-O3	2.355(3)
Dy1-O4	2.198(10)	Gd1-O4	2.259(12)
Dy1-O4	2.313(16)	Gd1-O4	2.321(12)
Dy1-O4'	2.45(2)	Gd1-O4'	2.41(2)
Dy1-O5	2.731(14)	Gd1-O5	2.692(10)
Dy1-N1	2.711(3)	Gd1-N1	2.724(3)
Dy1-N2	2.569(3)	Gd1-N2	2.587(3)

Dy1-N6	2.519(3)	Gd1-N6	2.554(3)
Select angles (º)			
Dy1-O4-Dy1	118.0(6)	Gd1-O4-Gd1	118.2(6)
Dy1-O4’-Dy1	108.12(6)	Gd1-O4’-Gd1	109.54(6)

Table S4: SHAPE constants for the Dy^{III} centers in **1a**. The lowest shape constants are bolded.

SHAPE Code	Point Group	Description	Dy1
EP-9	D_{9h}	Enneagon	35.468
OPY-9	C_{8v}	Octagonal pyramid	23.529
HBPY-9	D_{7h}	Heptagonal bipyramid	18.998
JTC-9	C_{3v}	Johnson triangular cupola J3	15.916
JCCU-9	C_{4v}	Capped cube J8	8.643
CCU-9	C_{4v}	Spherical-relaxed capped cube	8.304
JCSAPR-9	C_{4v}	Capped square antiprism	**0.691**
CSAPR-9	C_{4v}	Spherical capped square antiprism	**0.495**
JTCTPR-9	D_{3h}	Tricapped trigonal prism J51	2.647
TCTPR-9	D_{3h}	Spherical tricapped trigonal prism	1.686
JTDIC-9	C_{3v}	Tridiminished icosahedrons J63	11.938
HH-9	C_{2v}	Hula-hoop	11.634
MFF-9	C_s	Muffin	1.268

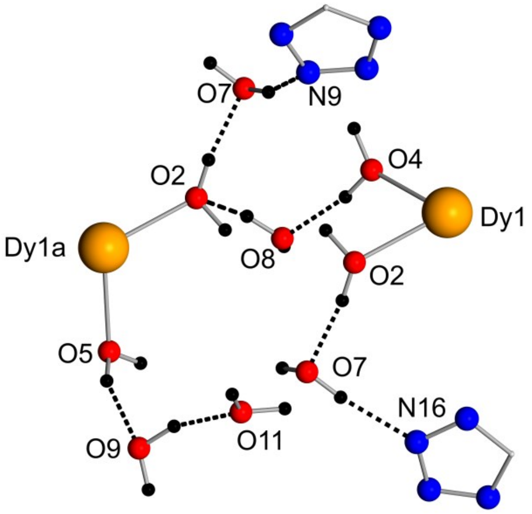

Fig. S1: Representative examples of hydrogen bonds formed in **1a** and **1b**, which includes both coordinated and lattice water molecules, as well as nitrogen atoms from the tetrazole moieties of the H_2TTP^{2-} ligand.

Table S5: SHAPE constants for the Dy^{III} centers in **2a** when coordinated to formate anions (9-coordinate). The lowest shape constant is bolded.

SHAPE Code	**Point Group**	**Description**	**Dy1**
EP-9	D_{9h}	Enneagon	32.537
OPY-9	C_{8v}	Octagonal pyramid	22.159
HBPY-9	D_{7h}	Heptagonal bipyramid	16.578
JTC-9	C_{3v}	Johnson triangular cupola J3	12.468
JCCU-9	C_{4v}	Capped cube J8	6.251
CCU-9	C_{4v}	Spherical-relaxed capped cube	6.026
JCSAPR-9	C_{4v}	Capped square antiprism	3.309
CSAPR-9	C_{4v}	Spherical capped square antiprism	**2.945**
JTCTPR-9	D_{3h}	Tricapped trigonal prism J51	3.110
TCTPR-9	D_{3h}	Spherical tricapped trigonal prism	3.126
JTDIC-9	C_{3v}	Tridiminished icosahedrons J63	11.950
HH-9	C_{2v}	Hula-hoop	8.883
MFF-9	C_s	Muffin	2.966

Table S6: SHAPE constants for the Dy^{III} centers in **2a** when coordinated to hydroxide anions (8-coordinate). The lowest shape constant is bolded.

SHAPE Code	**Point Group**	**Description**	**Dy1**
OP-8	D_{8h}	Octagon	29.645
HPY-8	C_{7v}	Heptagonal pyramid	24.568
HBPY-8	D_{6h}	Hexagonal pyramid	11.142
CU-8	O_h	Cube	6.955
SAPR-8	D_{4d}	Square antiprism	3.253
TDD-8	D_{2d}	Triangular dodecahedron	**2.088**
JGBF-8	D_{2d}	Johnson gyrobifastigium J26	11.878
JETBPY-8	D_{3h}	Johnson elongated triangular bipyramid J14	25.672
JBTPR-8	$C_{2\mathrm{v}}$	Biaugmented trigonal prism J50	2.669
BTPR-8	$C_{2\mathrm{v}}$	Biaugmented trigonal prism	2.142
JSD-8	D_{2d}	Snub diphenoid J84	5.148
TT-8	T_d	Triakis tetrahedron	7.798
ETBPY-8	D_{3h}	Elongated trigonal bipyramid	21.564

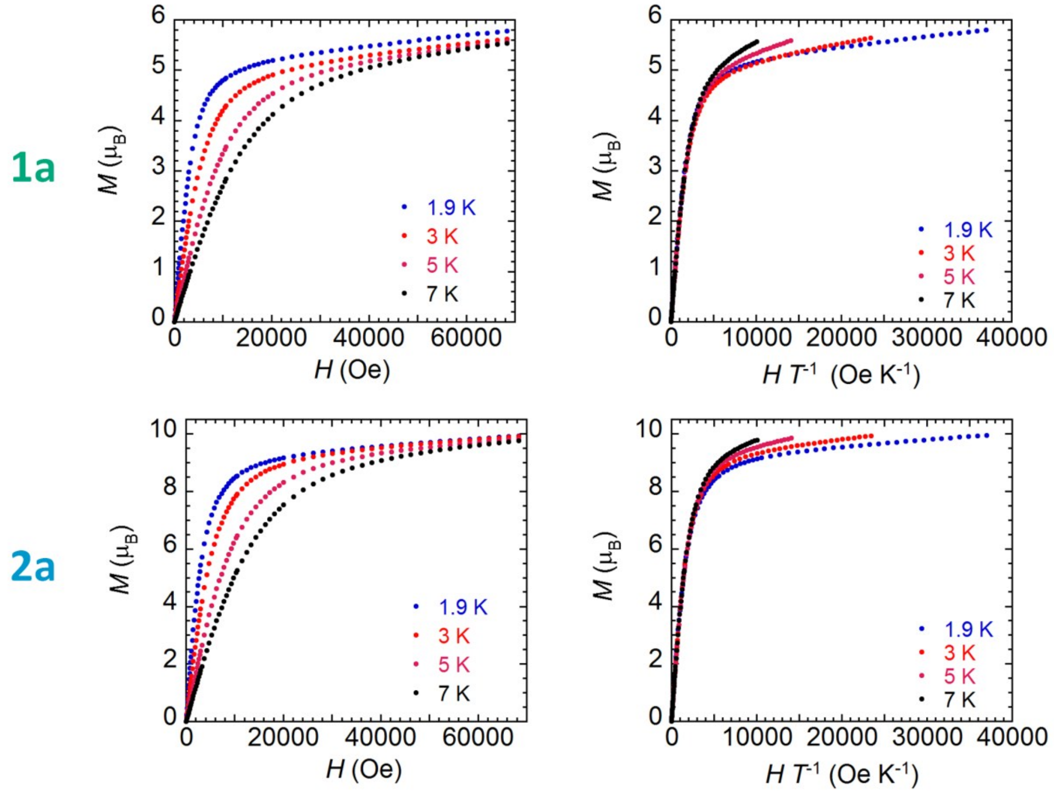

Fig. S2: Field dependence of the magnetization (left) and field dependence of reduced magnetization (right) at the indicated temperatures and up to 7 T for compounds **1a** and **2a**.

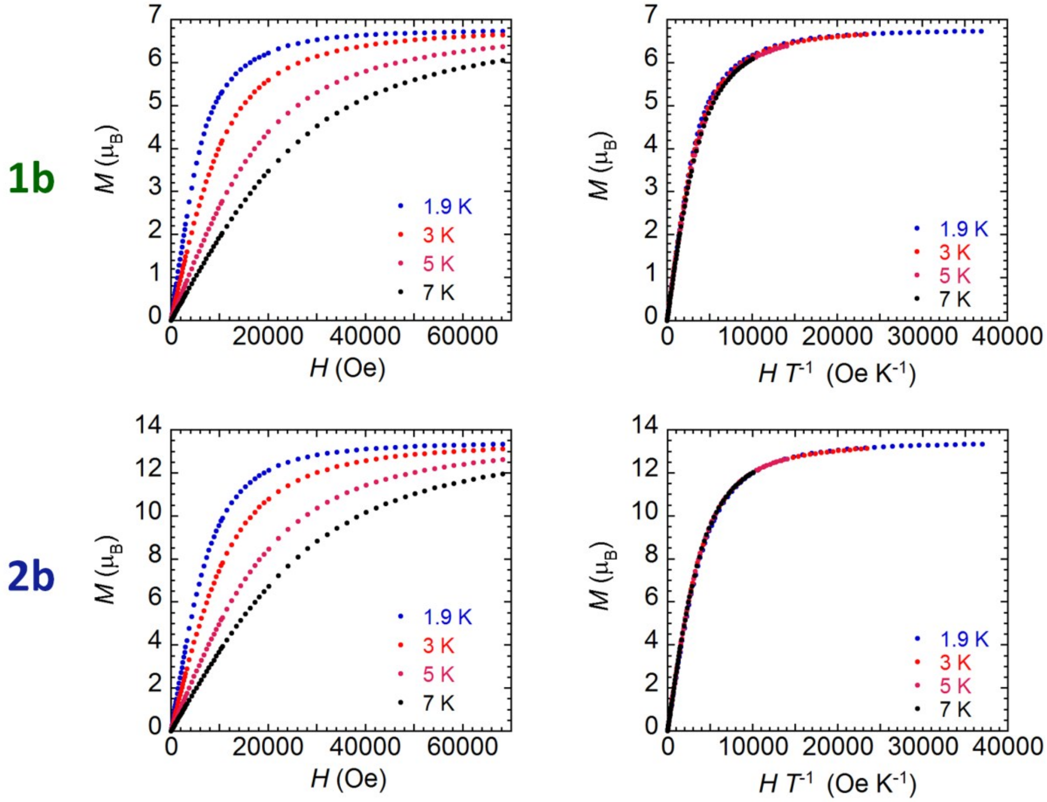

Fig. S3: Field dependence of the magnetization (left) and field dependence of reduced magnetization (right) at the indicated temperatures and up to 7 T for compounds **1b** and **2b**.

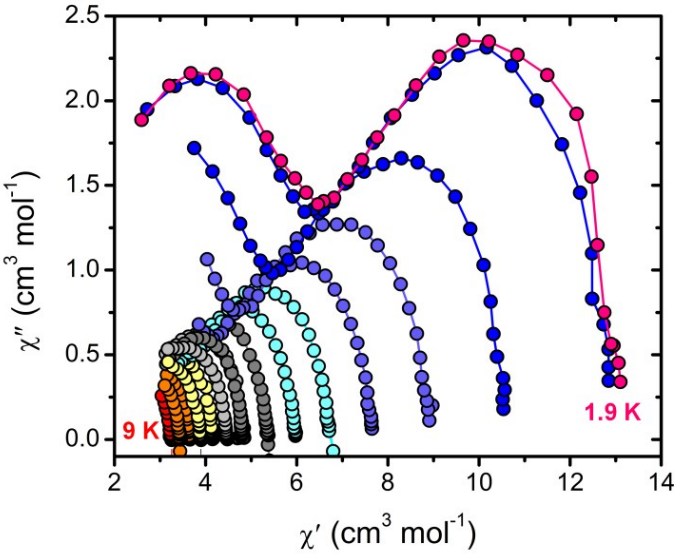

Fig. S4: Cole-Cole (Argand) plot for ac susceptibility data collected at 1000 Oe and varying temperatures for **1a**. Solid-lines are guides for the eyes.

Table S7: Values of the relaxation time (τ), α, χ_s and χ_T, for **1a** under a 1000 Oe dc field at varying temperatures. Red numbers indicate when values were restrained to remain physically reasonable (i.e. $\chi_s \geq 0$).

T (K)	τ (s)	α	χ_S	χ_T
1.9	0.0512(7)	0.152(8)	0.1696(2)	6.260(4)
2.0	0.0493(3)	0.153(1)	0.1590(5)	5.981(4)
2.5	0.0283(2)	0.230(3)	0.1038(9)	4.979(0)
3.0	0.0155(8)	0.290(6)	0.0859(7)	4.294(5)
3.5	0.0090(1)	0.303(1)	0.0798(3)	3.577(4)
4.0	0.0052(6)	0.303(8)	0.0521(1)	3.033(9)
4.5	0.0033(8)	0.286(1)	0.0238(2)	2.565(2)
5.0	0.0020(2)	0.256(4)	0.0127(8)	2.233(2)
5.5	0.0008(9)	0.296(1)	0.0127(8)	2.030(7)
6	0.0005(8)	0.320(9)	0.0052(1)	2.202(5)
6.5	0.0003(9)	0.269(2)	0.0033(7)	1.718(1)
7.0	0.0001(9)	0.291(9)	0.0013(1)	1.620(1)
7.5	0.0001(3)	0.243(8)	0	1.316(7)
8.0	0.0000982(2)	0.227(1)	0	1.166(8)
8.5	0.0000768(2)	0.175(8)	0	1.042(2)
9	0.0000349(7)	0.216(7)	0	1.041(2)

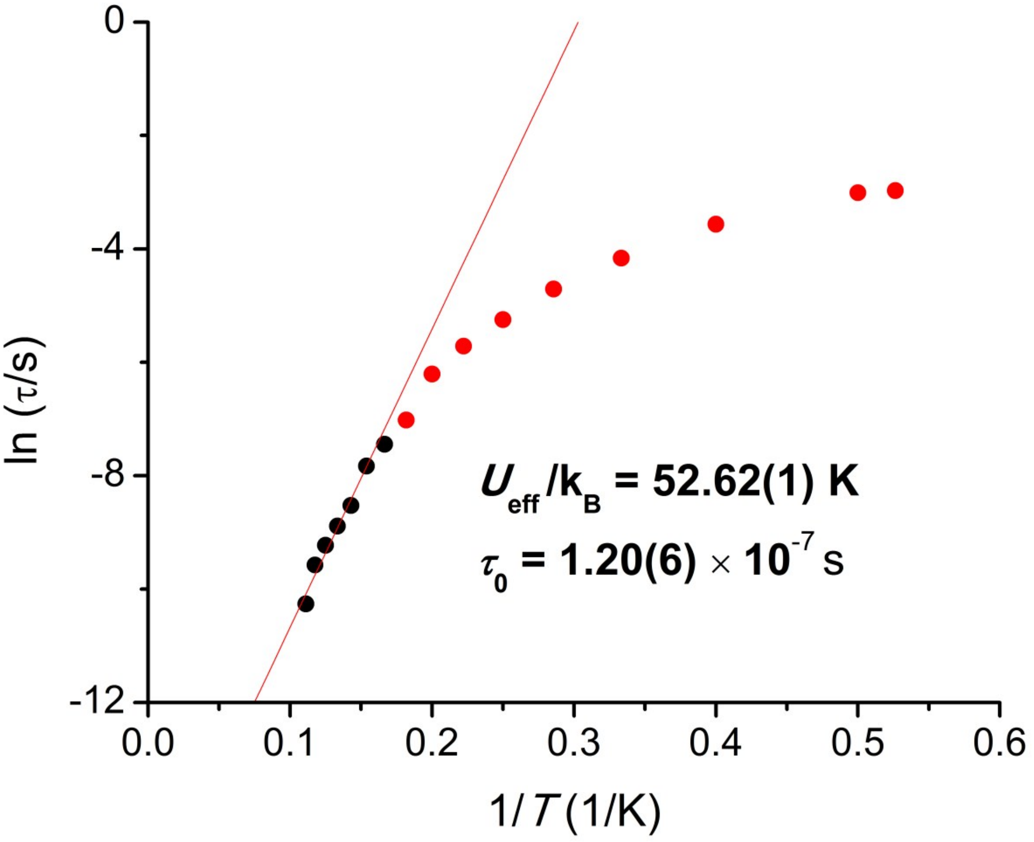

Fig. S5: Plot of ln (τ) versus 1/T for **1a** under an applied field of 1000 Oe.

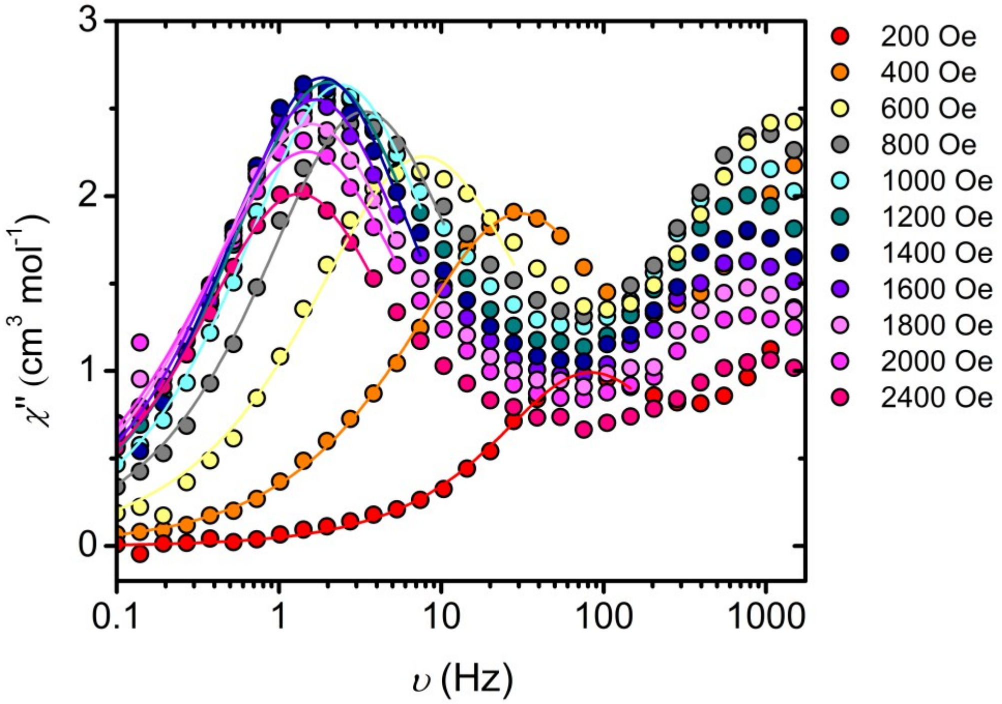

Fig. S6: Frequency dependence of the χ'' magnetic susceptibility for **1a** collected at 2 K and varying fields. The best-fit to the generalized Debye model are shown by colored lines.

Table S8: Values of the relaxation time (τ), α, χ_s and χ_T, for **1a** at 2 K under varying dc fields for the slow relaxation process. Red numbers indicate when values were restrained to remain physically reasonable (i.e. $\chi_s \geq 0$).

H (Oe)	**τ (s)**	**α**	**χ_S**	**χ_T**
200	0.0019(1)	0.127(9)	2.5994(6)	5.029(0)
400	0.0051(4)	0.234(4)	0.5235(7)	6.063(0)
600	0.0203(9)	0.231(0)	0.5074(0)	6.960(6)
800	0.0472(9)	0.184(2)	0.5916(1)	7.251(7)
1000	0.0657(4)	0.173(0)	0.5000(1)	7.440(9)
1200	0.0797(6)	0.174(4)	0.5037(6)	7.502(4)
1400	0.0857(1)	0.157(2)	0.5009(1)	7.371(0)
1600	0.0943(7)	0.172(9)	0.5026(1)	7.220(9)
1800	0.1010(8)	0.195(9)	0.5096(3)	7.104(0)
2000	0.107(4)	0.222(8)	0.5001(3)	6.945(6)
2400	0.119(6)	0.171(5)	0.6483(5)	5.935(4)

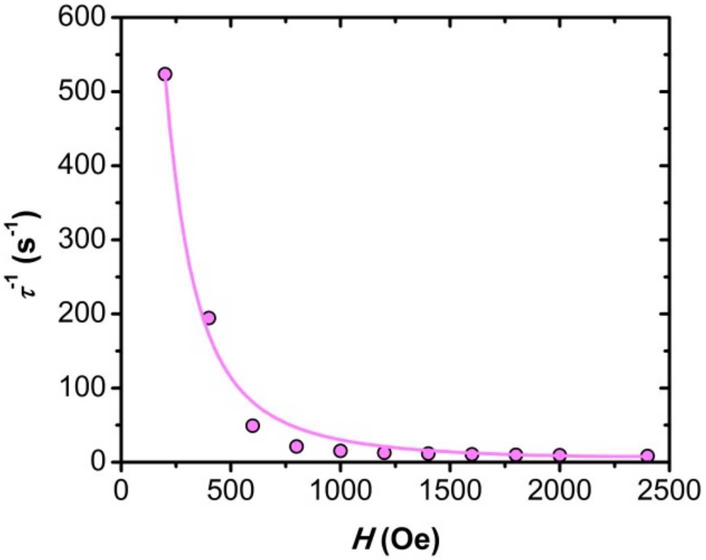

Fig. S7: Field dependence of the relaxation time for complex **1a**, plotted as τ^{-1} *vs* H and measured at 2 K. Solid line represents the best fit using the model described in the main text.

Table S9: Fitting parameters using eqn (2) for compound **1a**.

Parameter	Value
A (s^{-1} K^{-1} Oe^{-4})	2.91×10^{-14}
B_1 (s^{-1})	1563.16
B_2 (Oe^{-2})	4.99×10^{-5}
C (s^{-1} K$^{-8.18}$)	3.77×10^{-4}
τ_0 (s)	1.56×10^{-7}
U_{eff}/k_B (K)	42.06

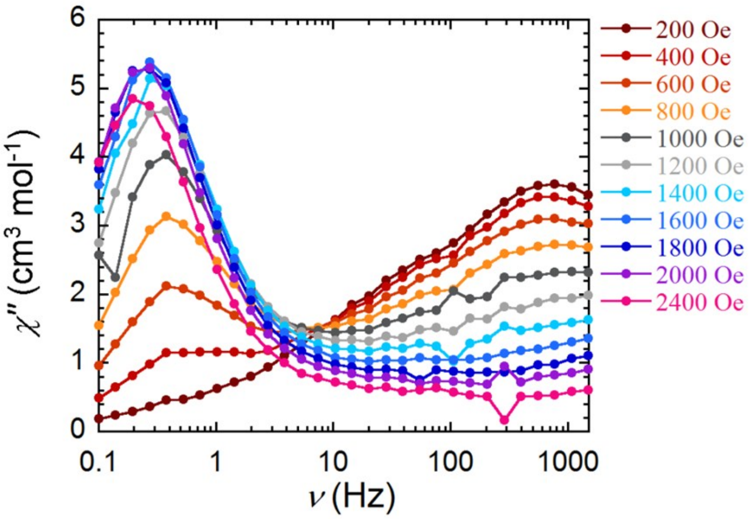

Fig. S8: Frequency dependence of the χ'' magnetic susceptibility for **2a** collected at 2 K and varying fields. Solid lines are guides for the eyes.

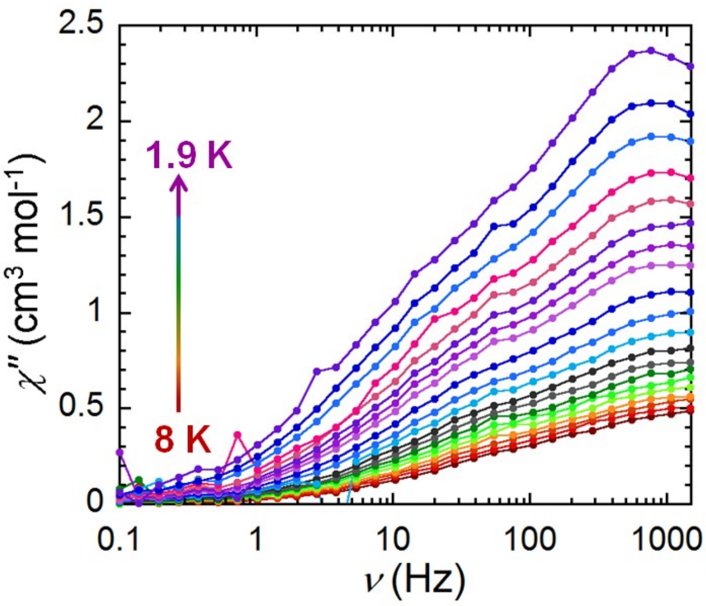

Fig. S9: Frequency dependence of the out-of-phase component of the ac susceptibility under zero applied field for compound **2a**.

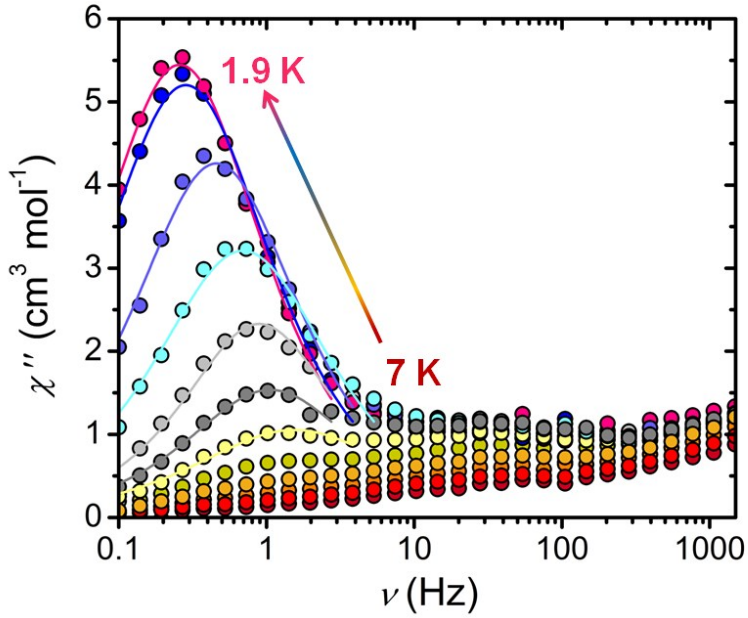

Fig. S10: Frequency dependence of the out-of-phase component of the ac susceptibility under an optimal magnetic dc field of 1600 Oe for **2a**.

Table S10: Values of the relaxation time (τ), α, χ_s and χ_T, for **2a** under a 1600 Oe dc field at varying temperatures.

T (K)	τ (s)	α	χ_S	χ_T
1.9	0.615(8)	0.099(7)	0.0158(4)	14.366(1)
2.0	0.561(0)	0.110(5)	0.0141(6)	12.401(1)
2.5	0.347(5)	0.0905(1)	0.0134(5)	9.828(0)
3.0	0.229(8)	0.118(6)	0.0114(2)	7.754(7)
3.5	0.178(4)	0.047(2)	0.0082(3)	6.410(7)
4.0	0.150(0)	0.103(9)	0.0075(0)	3.678(4)
4.5	0.102(9)	0.202(1)	0.0060(5)	2.982(9)

References

(1) APEX 2, Bruker AXS Inc., Madison, Wisconsin, USA.

(2) G. M. Sheldrick, SADABS, Program for empirical X-ray adsorption correction, BrukerNonius, 2004.

(3) G. M. Sheldrick, *Acta. Cryst. C*, 2015, **71**, 3.

(4) L. J. Farrugia, *J. Appl. Crystallogr.*, 1999, **32**, 837.

(5) Frisch M. J., Trucks G. W., Schlegel H. B., Scuseria G. E., Robb M. A., Cheeseman J. R., Scalmani G., Barone V., Mennucci B., Petersson G. A., Nakatsuji H., Caricato M., Li X., Hratchian H. P., Izmaylov A. F., Bloino J., Zheng G., Sonnenberg J. L., Hada M., Ehara M., Toyota K., Fukuda R., Hasegawa J., Ishida M., Nakajima T., Honda Y., Kitao O., Nakai H., Vreven T., Montgomery J. A. J., Peralta J. E., Ogliaro F., Bearpark M., Heyd J. J., Brothers E., Kudin K. N., Staroverov V. N., Kobayashi R., Normand J., Raghavachari K., Rendell A., Burant J. C., Iyengar S. S., Tomasi J., Cossi M., Rega N., Millam J. M., Klene M., Knox J. E., Cross J. B., Bakken V., Adamo C., Jaramillo J., Gomperts R., Stratmann R. E., Yazyev O., Austin A. J., Cammi R., Pomelli C., Ochterski J. W., Martin R. L., Morokuma K., Zakrzewski V. G., Voth G. A., Salvador P., Dannenberg J. J., Dapprich S., Daniels A. D., Farkas Ö., Foresman J. B., Ortiz J. V., Cioslowski J., J. F. D. *Gaussian 09, Revision E.01*, Gaussian, Inc., Wallingford CT, **2009**.

(6) Dennington R., Keith T., Millam J., *GaussView, Version 5*, Semichem Inc., Shawnee Mission, KS, USA, **2009**.